

Structural stability and aromaticity of pristine and doped graphene nanoflakes

Akira Akaishi^{1,2*}, Makoto Ushirozako^{1,2}, Haruyuki Matsuyama^{1,2}, and Jun Nakamura^{1,2†}

¹*Department of Engineering Science, The University of Electro-Communications(UEC-Tokyo), 1-5-1 Chofugaoka, Chofu, Tokyo 182-8585, Japan*

²*CREST, Japan Science and Technology Agency, 4-1-8 Honcho, Kawaguchi, Saitama 332-0012, Japan*

We have investigated quantitatively the relationship between the aromaticity and the structural stability of graphene nanoflakes (GNFs) using first-principles calculations. The aromaticity of each six-membered ring of GNFs is evaluated with the nucleus-independent chemical shifts (NICS). We have found that for armchair-edge GNFs, the degree of the stability, that is, the edge formation energy is proportional to the average of the NICS values for all six-membered rings. Even for nitrogen- and boron-doped GNFs, the average NICS values have strong correlation with the doping formation energies. Our results indicate that NICS is a good measure not only for the aromaticity but also for the structural stability of pristine/doped nano-graphene systems.

1. Introduction

Graphene, a two-dimensional material form of carbon atoms arranged in a honeycomb lattice, has attracted great attention because of its exceptional electronic and thermal properties.^{1–10)} Graphene nanoribbons (GNRs), a one-dimensional strip of graphene, and graphene nanoflakes (GNFs) have also received extensive attention as a promising candidate of next-generation materials for many applications.^{11–21)} Such nano-carbon materials are fabricated by several methods, *e.g.* a solution plasma technique.^{22,23)} Since GNFs are zero-dimensional materials, one of the key factors to determine their physical properties is their boundary, that is, shape and edges. It is known, both theoretically and experimentally, that the electronic and optical properties of GNFs vary depending on their size and shape of edges.^{24,25)} Kim *et al.* have successfully fabricated GNFs with various sizes up to 40 nm and have reported that the photoluminescence property of GNFs depends on their size.²⁶⁾ The shape of GNF edges also varies as the size changes. Relatively large scale GNFs of hexagonal shape can be fabricated on metal surfaces with

*E-mail address: akaishi@natori.ee.uec.ac.jp

†E-mail address: junj@ee.uec.ac.jp

use of C_{60} precursor.²⁷⁾ Although GNFs can be fabricated by several experimental techniques,²⁸⁾ it is difficult to precisely control the size and the edge shapes. Furthermore, it is not fully understood how the size and the edge shapes affect their stability.

To functionalize the graphene-based materials, it is important to modulate the electronic properties of graphene. One of the most common approaches to alter the electronic properties is doping of heteroatoms. It is reported that nitrogen/boron-doped graphene can be synthesized with the chemical vapor decomposition techniques.^{29,30)} The stability of doping into graphene systems has been extensively studied from the theoretical point of view.^{31,32)} It has been known that nitrogen/boron-doped graphene with uniform doping configuration is stabilized under a certain condition, which can be understood through the symmetry of doping configurations and its electronic structures.³³⁾ For GNRs, the edge shape is relevant to the stability of heteroatom doping. In particular, the edge-localized states appearing on zigzag edges play a crucial role on the doping stability.^{34–36)} For the nitrogen doping, a valence electron of the nitrogen atom occupies an unoccupied edge state, while the other four valence electrons form three sp^2 - σ bondings and π -conjugated network with neighboring carbon atoms. For boron doped systems, *vice versa*, the occupied edge state on zigzag edges localizes on the boron atom to form the π -conjugated rings. In other words, a “hole” induced by the boron atom doping occupies the edge states. The stabilization mechanism of heteroatom doping can be understood by the charge transfer between dopants and the edge states.³⁶⁾ Hence, the charge redistribution with doping dominates the doping stability as well as the edge shape.

The stability and the reactivity of polycyclic aromatic hydrocarbons (PAHs) have been discussed with an idea of the aromaticity.^{37–39)} The well-known Hückel’s rule describes the stability of PAHs with $(4n+2)$ π -electrons that are delocalized around six-membered rings.^{37,40)} More advanced understanding of the aromaticity was developed by Clar on the basis of the resonance of π electrons.^{39,41)} The Clar formula describes the method to determine which six-membered rings of PAHs are aromatic in accordance with the resonance of the so-called Kekulé structure. The PAHs with the Clar-sextets become stable owing to the resonance energy of π electrons.

In recent decades, several theoretical methods have been developed to evaluate the aromaticity of the six-membered rings of PAHs within the framework of the molecular orbital theory. One of the most reliable measures for the ring aromaticity is the nucleus-independent chemical shifts (NICS), developed by Schleyer.⁴²⁾ The concept of NICS

is based on magnetic shielding of external magnetic fields, which is induced by the existence of ring currents within cyclic structures of a molecule. In fact, for many polycyclic chemical compounds including PAHs, it has been reported that the aromatic rings in terms of NICS values correspond to the Clar's π -sextets.^{43–45)}

The aromaticity is also relevant to chemical reactivity and the stability of the molecules. Aihara has developed the framework to evaluate the resonance energy of each six-membered rings of PAHs.⁴⁶⁾ Using the resonance energy-based method, the pattern of which rings are resonant illustrates the spatial map of aromatic rings in the Clar structure.^{47–49)} Indeed, the energetic analyses based on the resonance energy have revealed that the Clar structure is relevant to the aromatic stability of cyclic compounds. In addition, the relation between the aromaticity in terms of the Clar structure and the structural stability has been discussed by investigating the electronic structures of relatively large GNFs using the density functional theory (DFT) calculations.⁵⁰⁾ For such GNFs, the electronic structures of the highest occupied molecular orbitals (HOMOs) and the lowest unoccupied molecular orbitals (LUMOs) play a significant role to determine the structural stability as well as the energy gap between HOMO and LUMO.

Among these previous studies, however, the quantitative understanding of the relationship between the aromaticity and the structural stability is limited. Furthermore, the aromaticity of doped graphene systems has not been discussed so far. In the present paper, we discuss the structural stability of GNFs and doped GNFs in view of aromaticity. In particular, we focus on the relationship between the NICS value and the formation energy. For doped GNFs, we investigate the local electronic structure around dopant atoms and how the change of the charge distribution by the doping affects the NICS values.

2. Calculation Models and Methods

We calculated the stability and the aromaticity of the following models: (i) the hexagonal GNFs (h -GNFs), (ii) the triangular GNFs (t -GNFs), (iii) the rhombic GNFs (r -GNFs), and (iv) the nitrogen/boron-doped hexagonal GNFs. As shown in Fig. 1, we consider the h -GNFs with both the zigzag (ZZ) and armchair (AC) edges. The chemical formulae for zigzag-edge h -GNFs (ZZGNFs), t -GNFs, and r -GNFs are $C_{6n^2}H_{6n}$, $C_{3n(n+1)}H_{6n}$, and $C_{6n^2}H_{2(4n-1)}$, respectively. The armchair-edge h -GNFs are classified into two types, namely AC1 and AC2 types, where the chemical formulae are

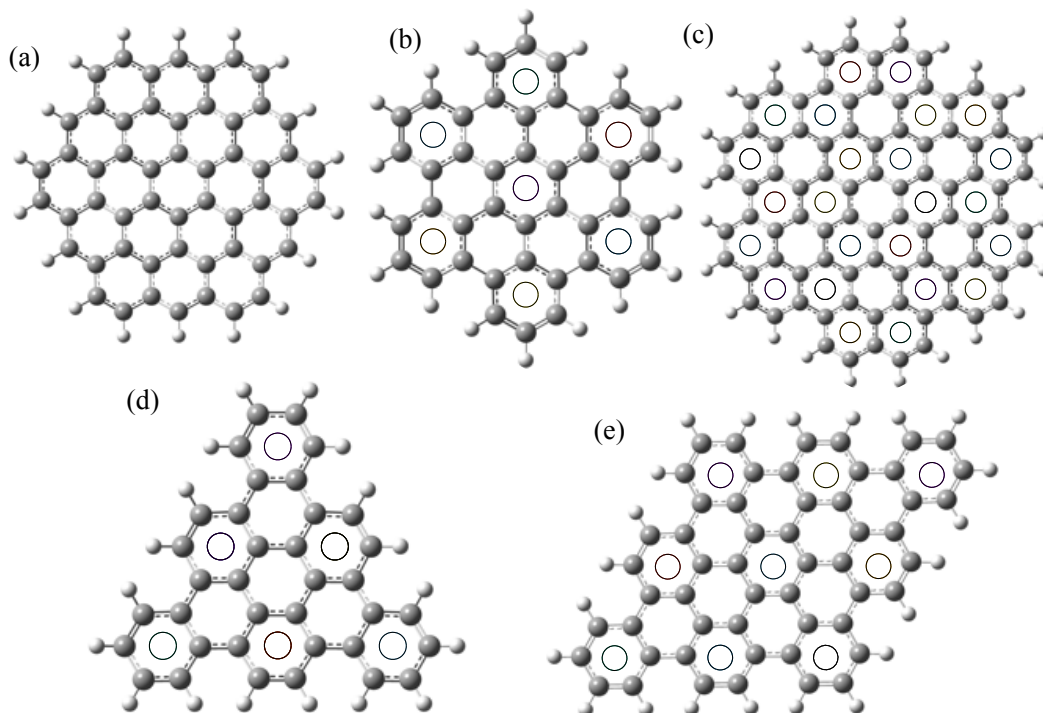


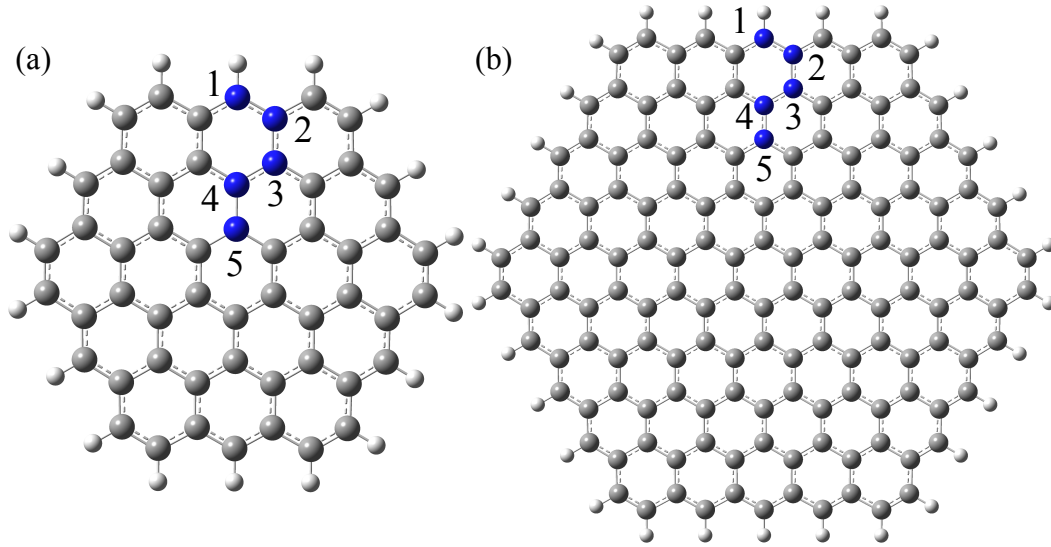
Fig. 1. Models for (a) $C_{54}H_{18}$ (ZZGNF), (b) $C_{42}H_{18}$ (AC1GNF), (c) $C_{84}H_{24}$ (AC2GNF), (d) $C_{36}H_{18}$ (*t*-GNF), and (e) $C_{54}H_{22}$ (*r*-GNF). Gray and white balls indicate carbon and hydrogen atoms, respectively. Black circles indicate the Clar's π -sextets. The Clar's sextets are defined so that (i) Kekulé resonance structures do not lie next to each other and (ii) the number of the resonant rings is maximized. For AC2GNFs, two identical Clar structures are depicted. The detail description of the Clar structure can be found in Ref.⁴¹⁾

$C_{18n^2-18n+6}H_{12n-6}$ and $C_{18n^2-30n+12}H_{12n-12}$, respectively. Note that the AC1 type GNFs (AC1GNFs) have one carbon atom on each vertex of the envelope hexagon, while the AC2 type GNFs (AC2GNFs) have two carbon atoms (see Fig. 1). For *t*-GNFs and *r*-GNFs, we only considered those with armchair edges. The point groups of *h*-GNFs, *t*-GNFs, and *r*-GNFs are D_{6h} , D_{3h} , and D_{2h} , respectively. The chemical compositions of the models employed in the present study are listed in Table I.

We also considered the doped GNFs where one carbon atom is substituted by a nitrogen or boron atom. Figure 2 shows the calculation models of the heteroatom-doped GNFs. Nitrogen and boron atoms are preferably doped at the zigzag edges of graphene because of the existence of the so-called edge states.³⁶⁾ Our doped GNFs consist of the *h*-GNFs with zigzag edges and the dopant atom is placed in the middle of the edge. We calculated several doping sites by changing the distance from the edge (see Fig. 2).

Table I. List of the models employed. For the AC type GNFs, the purities (see text) are also indicated.

ZZ	<i>h</i> -GNFs		<i>t</i> -GNFs	<i>r</i> -GNFs
	AC1 (purity)	AC2 (purity)		
C ₂₄ H ₁₂			C ₃₆ H ₁₈	C ₅₄ H ₂₂
C ₅₄ H ₁₈	C ₄₂ H ₁₈ (0.667)	C ₈₄ H ₂₄ (0.5)	C ₆₀ H ₂₄	C ₉₆ H ₃₀
C ₉₆ H ₂₄	C ₁₁₄ H ₃₀ (0.8)	C ₁₈₀ H ₃₆ (0.667)	C ₉₀ H ₃₀	C ₁₅₀ H ₃₈
C ₁₅₀ H ₃₀	C ₂₂₂ H ₄₂ (0.857)	C ₃₁₂ H ₄₈ (0.75)	C ₁₂₆ H ₃₆	C ₂₁₆ H ₄₆
C ₂₁₆ H ₃₆	C ₃₆₆ H ₅₄ (0.889)	C ₄₈₀ H ₆₀ (0.8)	C ₁₆₈ H ₄₂	
C ₂₉₄ H ₄₂	C ₅₄₆ H ₆₆ (0.909)	C ₆₈₄ H ₇₂ (0.833)		
C ₃₈₄ H ₄₈	C ₇₆₂ H ₇₈ (0.923)	C ₉₂₄ H ₈₄ (0.857)		
C ₄₈₆ H ₅₄	C ₁₀₁₄ H ₉₀ (0.933)	C ₁₂₀₀ H ₉₆ (0.875)		
C ₆₀₀ H ₆₀				

**Fig. 2.** Model of the doped GNFs. (a) C₅₃XH₁₈, (b) C₁₄₉XH₃₀ (X=N,B). Blue balls indicate dopant atoms, where each doping configuration is labeled by numbers.

The structural stability of non-doped GNFs was evaluated on the basis of the edge formation energy, E_{edge} defined as

$$E_{\text{edge}} = \frac{1}{n_{\text{H}}}(E_{\text{GNF}} - n_{\text{C}}E_{\text{C}} - n_{\text{H}}\mu_{\text{H}}), \quad (1)$$

where E_{GNF} is the total energy of GNFs and E_{C} is the total energy per atom of pristine graphene. n_{C} and n_{H} are the numbers of C and H atoms, respectively. μ_{H} is the chemical

potential of a hydrogen atom, which is given as

$$\mu_{\text{H}} = \frac{1}{6}(E_{\text{benzene}} - 6E_{\text{C}}), \quad (2)$$

where E_{benzene} is the total energy of benzene. As for the stability of the doped GNFs, we have calculated the formation energy for the substitutional doping,

$$E_{\text{dope}} = (E_{\text{N(B)}} + E_{\text{C}}) - (E_{\text{GNF}} + \mu_{\text{N(B)}}), \quad (3)$$

where $E_{\text{N(B)}}$ is the total energy of the N(B)-doped GNFs and $\mu_{\text{N(B)}}$ is the chemical potential of N(B). In the present study, we adopted the energy per atom of a nitrogen molecule and of a B₁₂ cluster for μ_{N} and μ_{B} , respectively.

For DFT calculations, we used the GAUSSIAN09 program package⁵¹⁾ employing the local spin density approximation with the VWN functional⁵²⁾ and the 6-31G basis set in the package. We also used the 6-31G(d,p) basis set for doped systems and found no qualitative change of results (see the supplementary data). Structural optimization with respect to ionic positions was performed until each component of the interatomic force becomes less than 0.0003 Ha/Bohr. Aromaticity of a given ring was evaluated by the NICS(1) values that was a NICS value at the point 1 Å above the center of the ring. Note that significantly negative NICS values indicate the aromaticity of the ring and rings with positive values are antiaromatic. All doped systems kept the structure planar during the optimization and no buckled structures of dopants were observed.

3. Results and discussion

3.1 Stability and aromaticity of non-doped GNFs

Figure 3 shows the edge formation energies of *h*-GNFs as a function of the number of carbon atoms at the edges. For ZZGNFs, the formation energy per edge atom increases with increasing size of GNF. The formation energies for ACGNFs saturate for the large GNFs. Note that there is a distinct difference between AC1 and AC2 in the stability, where AC2GNFs are more stable than AC1GNFs. Contrary to the ACGNFs, the edge of ZZGNFs becomes unstable as the size of GNF becomes large. This is due to the existence of the edge-localized state: as well as the GNRs with zigzag edges,¹⁷⁾ the states localized at the zigzag edges make the system unstable. In fact, the HOMOs of ZZGNFs have large amplitude at the edges (see Fig. 4). Such localization of HOMOs becomes prominent as the size of the edge increases. The edge states apparently emerge at the edges of ZZGNFs larger than C₉₆H₂₄. Accordingly, the formation energies of ZZGNFs deviate from the trends of those of ACGNFs at C₉₆H₂₄ (see Fig. 3). Thus, the

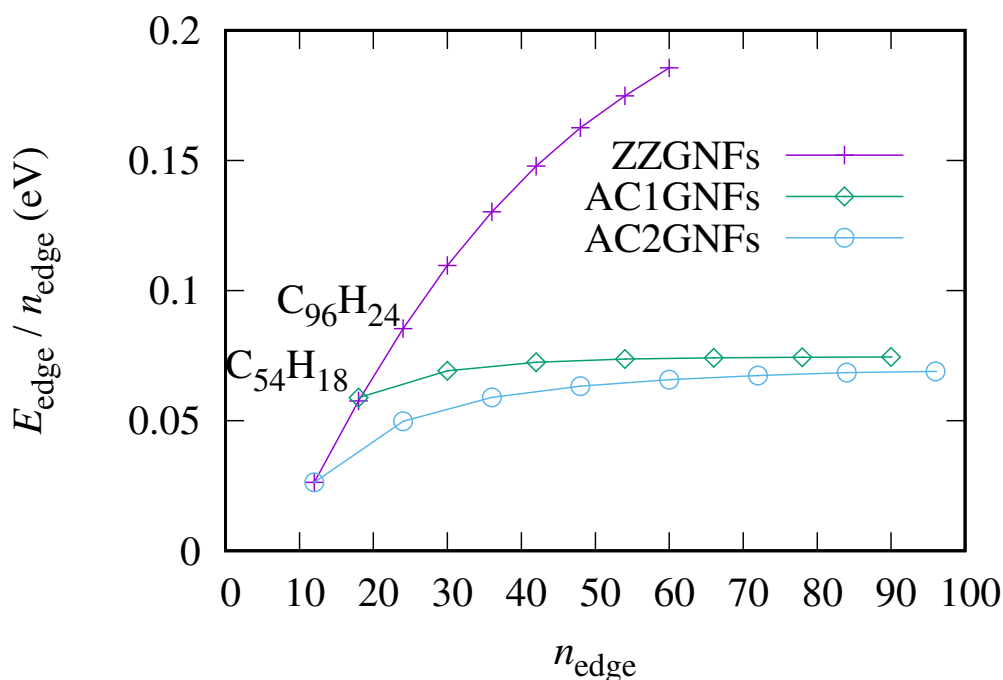


Fig. 3. Edge formation energies per edge atom as a function of the number of edge atoms, n_{edge} . The formation energies for ZZGNFs, AC1GNFs, and AC2GNFs are indicated by crosses, diamonds, and circles, respectively.

instability of ZZGNFs is attributed to the evolution of the edge state.

We presume that the edge formation energies for ZZGNFs also saturate for larger sizes. If the size of edges is large enough, the edge states dominate the edge stability and the effects of flake corners become negligible. As a result, the stability of large GNFs is attributed only to the difference in edge types. For GNRs, the formation energy per edge atom of the zigzag edge is larger by 0.2 eV than that for the armchair edge.¹⁷⁾ The saturated formation energy for ZZGNFs is estimated to be 0.275 eV and the edge size n_{edge} required for the saturation is about 250.

For the stability of ACGNFs, the AC2 type GNFs are more stable than the AC1 type in any edge size. This observation is somewhat counterintuitive: At the vertices of the envelope hexagon of AC1GNFs, the corner consists of one carbon atom, while there are two carbon atoms at those of AC2GNFs. We here define that the pure AC type carbon atom on edges is a carbon atom bonded with a hydrogen atom for which only one of the neighboring carbon atoms is also bonded with a hydrogen atom and the second neighboring carbon atoms have no bonds with hydrogen atoms. One can

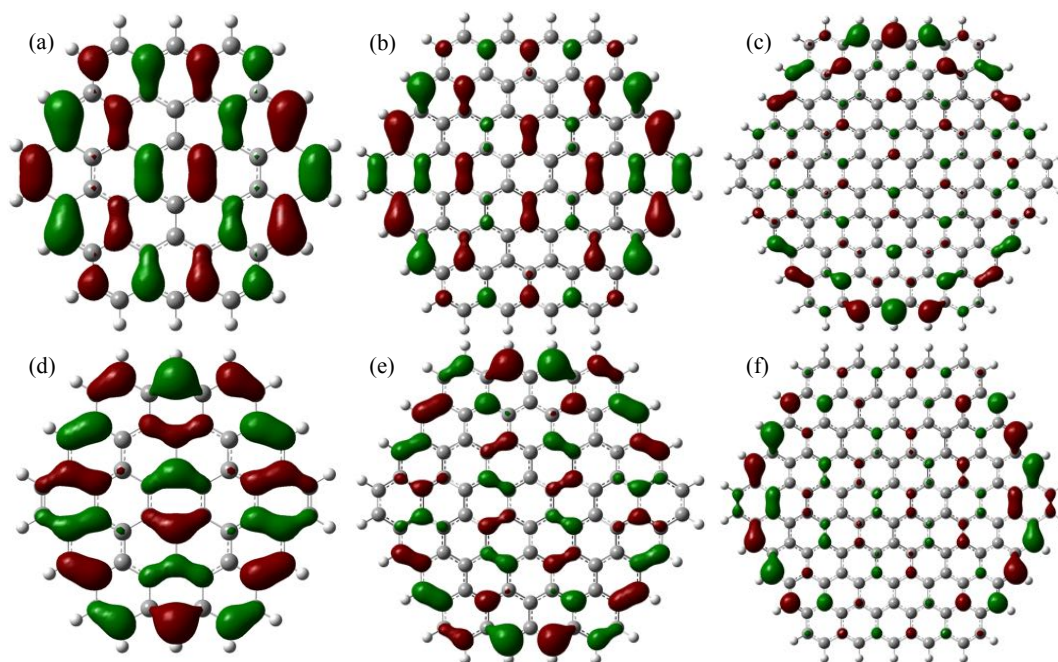


Fig. 4. Isosurfaces of HOMOs for (a, d) $C_{54}H_{18}$, for (b, e) $C_{96}H_{24}$, and for (c, f) $C_{150}H_{30}$. HOMOs consist of doubly-degenerate orbitals.

check that the corner carbon atoms do not satisfy this definition and thus AC1GNFs (AC2GNFs) have one (two) impure AC type carbon atom(s). The ratio of the number of the pure AC atoms to that of the edge atoms is defined as the purity of the AC edge.

The AC purities for AC1 and AC2 GNFs are listed in Table I. The purity of AC1GNFs is greater than that of AC2GNFs. In view of the AC purity, one may expect that AC2GNFs are more likely to have the edge properties of ZZGNFs than AC1GNFs. Consequently, AC2GNFs are expected to be unstable than AC1GNFs, since zigzag edges are energetically unstable. However, this is not the case for the observed trend of the edge formation energies, indicating that the stability of ACGNFs is not necessarily dominated by the edge type.

We investigate the difference in the stability between AC1GNFs and AC2GNFs in view of the aromaticity. Figure 5 depicts the color maps of NICS values for each six-membered ring. For AC1GNFs, the six-membered ring at the flake center has the negatively-largest NICS value and the NICS values of the neighboring rings are close to zero. The 2nd neighbor rings of the center ring have small NICS values. The rings with large NICS values can be distinguished as the Clar's π sextets and this spatial arrangement corresponds to the Clar structure as shown in Fig. 1 (b). On the other hand, for AC2GNFs, the NICS value of the center ring is small and the neighboring

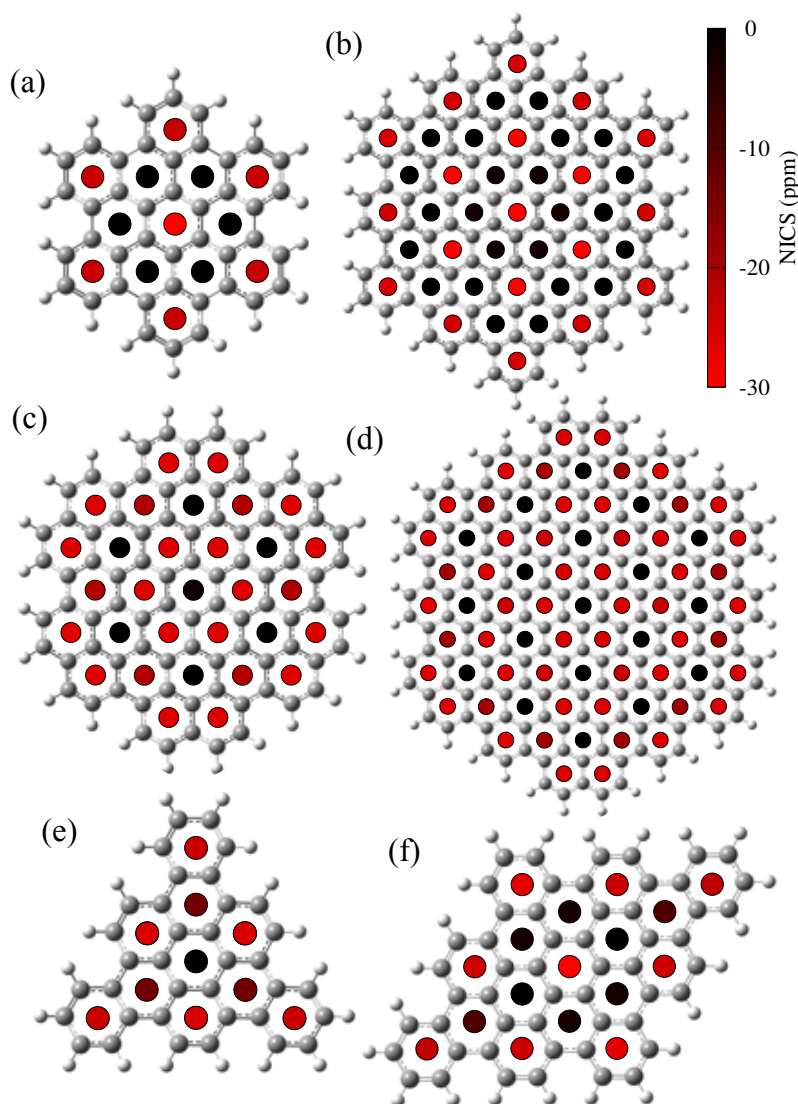


Fig. 5. Color maps of the NICS values for (a) $C_{42}H_{18}$, (b) $C_{114}H_{30}$, (c) $C_{84}H_{24}$, (d) $C_{180}H_{36}$, (e) $C_{36}H_{18}$, and (f) $C_{54}H_{22}$. The NICS values for the other molecules are found in the supplementary data.

rings large. This pattern for AC2 again coincides the Clar structure (see Fig. 1 (c)). Such coincidence has also been discussed in the literature.^{44,45)} We emphasize that this correspondence between the patterns of NICS values and the Clar structure is also found for all *t*-GNFs and *r*-GNFs (see Fig. 1 (d,e) and Supplementary data).

While the relation between the aromaticity in terms of NICS calculations and the Clar structure has been discussed so far, however, a quantitative relationship has not been fully understood. To this end, we relate the stability to the aromaticity by means

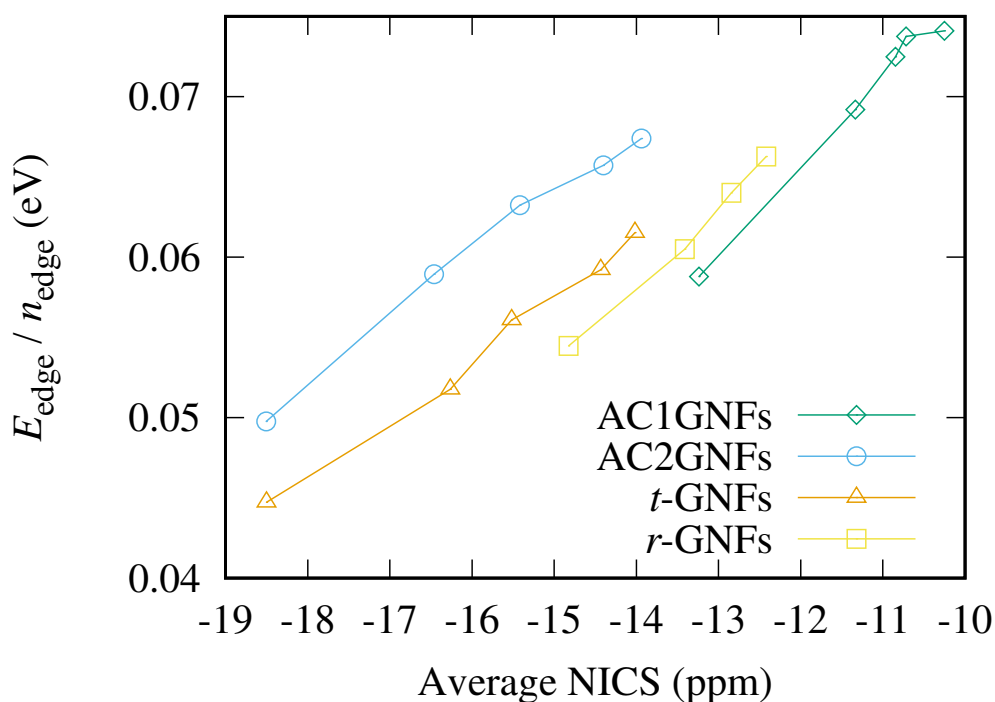


Fig. 6. Edge formation energy per edge atom versus the average NICS values. The formation energies for AC1GNFs, AC2GNFs, t -GNFs, and r -GNFs are indicated by the diamonds, circles, triangles, and squares, respectively.

of NICS values averaged over all six-membered rings of a GNF. Figure 6 shows the relationship between the edge formation energies and the average NICS values. In addition to ACGNFs, we calculated those for t -GNFs and r -GNFs. As clearly seen, the edge formation energy is proportional to the average NICS value. The slope is almost the same for each type of GNFs and the intercept depends on the type. The average NICS values have one-to-one correspondence with the formation energy regardless of the GNF size. This means that the stability of the GNF edge is dominated by the degree of the aromaticity over the whole rings of GNFs. Therefore, it is concluded that the NICS values are not just the measure of aromaticity but also are relevant to the structural stability of GNFs.

3.2 Doped GNFs

As shown in the previous sections, the NICS values successfully predict the Clar structure, that is, the local aromaticity of GNFs, thus become a good measure of the stability of GNFs. However, one can not apply the Clar structure to heteroatom doped systems, since the types of bonding between dopant and neighboring carbon atoms are not always

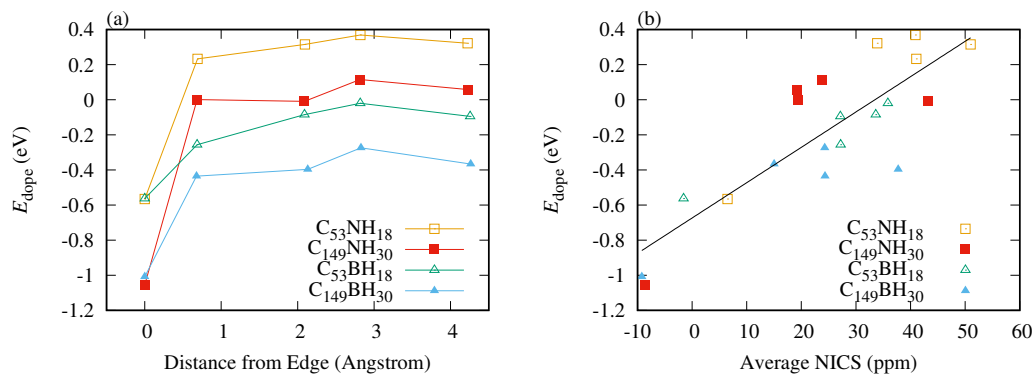


Fig. 7. (a) Dope formation energies for the nitrogen- and boron-doped GNFs as a function of the distance between the dopant and the edge. (b) E_{dope} versus the average NICS values. The black line is a line of the least square fitting. The correlation coefficient for the data is 0.8415. The doping energies for $C_{53}NH_{18}$, $C_{53}BH_{18}$, $C_{149}NH_{30}$, and $C_{149}BH_{30}$ are indicated by open squares, open triangles, filled squares, and filled triangles, respectively.

uniquely determined. Here, we examine the relationship between the aromaticity and the structural stability for nitrogen- and boron-doped GNFs. Since nitrogen and boron atoms are preferably doped at zigzag edges,³⁶⁾ we have considered doped ZZGNFs. The stability of doped GNFs is discussed by means of the formation energy for doping. Figure 7(a) shows the dope formation energies as a function of the distance between a doping site and the zigzag edge. For both nitrogen and boron dopings, the formation energy increases with increasing distance from the edge. Furthermore, the formation energies for $C_{149}XH_{30}$ ($X=N,B$) are smaller than those for $C_{53}XH_{18}$ for the same doping configuration. These results are associated with the emergence of the edge state at the zigzag edge: As discussed in the previous sections, the HOMOs for $C_{150}H_{30}$ are clearly localized at the zigzag edges. Such formation of the edge state contributes to the stabilization of heteroatom doping, for the nitrogen and boron doping in GNRs, as discussed in the literature.^{34–36,53)}

The charge redistribution caused by the localization/delocalization of the edge states affects the aromaticity of the rings around the dopant atom. In order to elucidate the aromaticity for the doped systems, we show the NICS patterns for the nitrogen-doped ZZGNF in Fig. 8. The NICS values of the rings around the nitrogen atom are positive, meaning that these rings are antiaromatic. As for the doping sites distant from the edge, there are several antiaromatic rings around the dopant. The rings which are distant from the dopant remain aromatic. This observation clearly indicates that the charge redistribution around the dopant makes the neighboring rings antiaromatic. It is noted

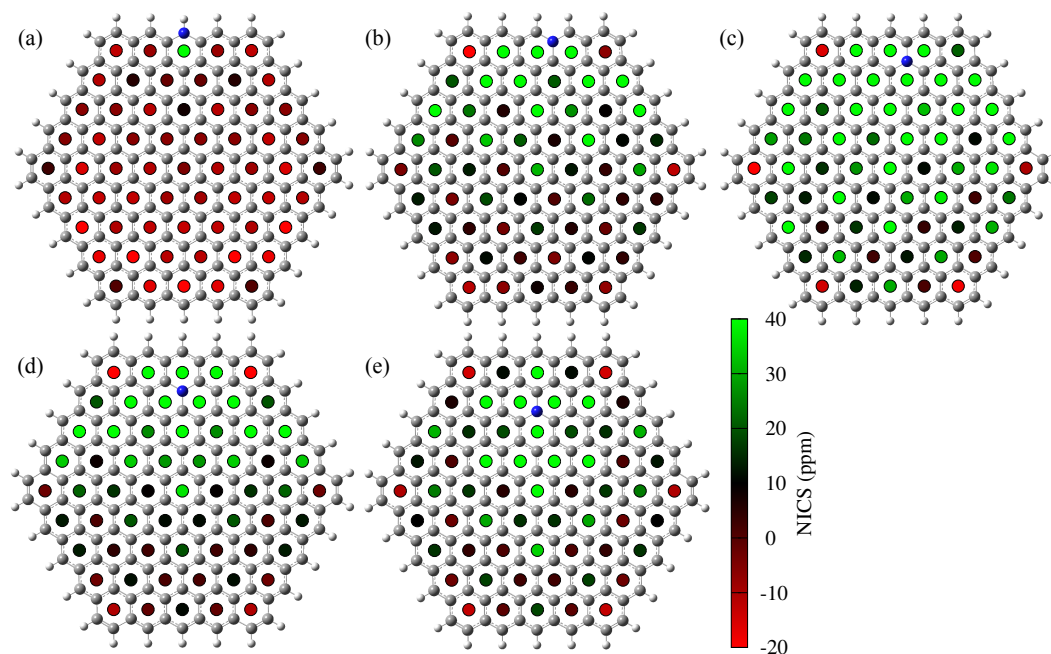


Fig. 8. Color maps of the NICS values of $C_{149}NH_{30}$ where the dopant position is 1, 2, 3, 4, and 5 for (a), (b), (c), (d), and (e), respectively.

that for the site-1 doping, as shown in Fig. 8(a), only the six-membered ring containing the nitrogen atom becomes antiaromatic and the others are hardly affected by the doping [see the NICS patterns for non-doped ZZGNFs in Fig. S1(c)]. This accords with the fact that the charge redistribution is limited to take place at the edge, if the N or B atom is doped just at the edge.³⁶⁾ Since it is known that the distribution of the dopant charge is closely related to the stability of the doped systems,³⁶⁾ the aromaticity should be also related to the stability. In fact, for the doped ZZGNFs, the doping stability has strong correlations with the NICS values. Figure 7(b) shows the relation between the dope formation energy and the average NICS value. As clearly seen in this figure, these two measures are correlated with each other as well as the non-doped GNFs. It should be addressed that the NICS value is a good measure not only for the aromaticity but also for the stability in the π -conjugated systems even containing nitrogen and boron atoms.

4. Conclusions

We have examined the stabilities of GNFs and doped GNFs and related them to the aromaticity by means of NICS values. The stability of non-doped GNFs is dominated by the following factors: (i) The formation of zigzag edges make GNFs unstable because

of the existence of the edge states. (ii) The average NICS values have a strong correlation with the structural stability regardless of the shape of GNFs. For both nitrogen- and boron-doped GNFs, the dopant atom is preferably doped near the zigzag edges. This is because the electron/hole from the nitrogen/boron atom migrates to the unoccupied/occupied edge states. Even for doped GNFs, the average NICS values have positive correlation with the doping formation energy, whereas the six-membered rings around the dopant become antiaromatic.

The Clar formula is useful to describe the resonance structure of PAHs in terms of the aromaticity. As for doped systems, however, it is not always valid to predict the aromatic rings using the Clar formula, since the number of π electrons for dopants and neighboring carbon atoms is not necessarily predictable unlike non-doped carbon systems. In spite of the lack of the Clar structure, for the nitrogen- and boron-doped ZZGNF systems, the NICS value is certainly a good measure to predict the structural stability. It has been clarified that the aromaticity is relevant to the stability not only for GNFs but also for doped GNFs, where the Clar formula is necessarily applicable.

References

- 1) K. S. Novoselov, A. K. Geim, S. V. Morozov, D. Jiang, Y. Zhang, S. V. Dubonos, I. V. Grigorieva, and A. A. Firsov, *Science* **306**, 666 (2004).
- 2) K. Saito, J. Nakamura, and A. Natori, *Phys. Rev. B* **76**, 115409 (2007).
- 3) K. Bolotin, K. Sikes, Z. Jiang, M. Klima, G. Fudenberg, J. Hone, P. Kim, and H. Stormer, *Solid State Commun.* **146**, 351 (2008).
- 4) A. A. Balandin, S. Ghosh, W. Bao, I. Calizo, D. Teweldebrhan, F. Miao, and C. N. Lau, *Nano Lett.* **8**, 902 (2008).
- 5) S. Ghosh, I. Calizo, D. Teweldebrhan, E. Pokatilov, D. Nika, A. Balandin, W. Bao, F. Miao, and C. Lau, *Appl. Phys. Lett.* **92**, 151911 (2008).
- 6) Y. Yokomizo and J. Nakamura, *Appl. Phys. Lett.* **103**, 113901 (2013).
- 7) J. Nakamura and A. Akaishi, *Jpn. J. Appl. Phys.* **55**, 1102A9 (2016).
- 8) Y. Zhang, Y.-W. Tan, H. L. Stormer, and P. Kim, *Nature* **438**, 201 (2005).
- 9) K. S. Novoselov, Z. Jiang, Y. Zhang, S. V. Morozov, H. L. Stormer, U. Zeitler, J. C. Maan, G. S. Boebinger, P. Kim, and A. K. Geim, *Science* **315**, 1379 (2007).
- 10) C. L. Kane and E. J. Mele, *Phys. Rev. Lett.* **95**, 226801 (2005).
- 11) M. Fujita, K. Wakabayashi, K. Nakada, and K. Kusakabe, *J. Phys. Soc. Jpn.* **65**, 1920 (1996).
- 12) K. Wakabayashi, M. Fujita, H. Ajiki, and M. Sigrist, *Phys. Rev. B* **59**, 8271 (1999).
- 13) B. Huang, *Phys. Lett. A* **375**, 845 (2011).
- 14) M. Terrones, A. R. Botello-Méndez, J. Campos-Delgado, F. López-Urías, Y. I. Vega-Cantú, F. J. Rodríguez-Macías, A. L. Elías, E. Muñoz-Sandoval, A. G. Cano-Márquez, J.-C. Charlier, *et al.*, *Nano Today* **5**, 351 (2010).
- 15) G. Lee and K. Cho, *Phys. Rev. B* **79**, 165440 (2009).
- 16) Z. Guo, D. Zhang, and X.-G. Gong, *Appl. Phys. Lett.* **95**, 163103 (2009).
- 17) S. Okada, *Phys. Rev. B* **77**, 041408 (2008).
- 18) Y.-W. Son, M. L. Cohen, and S. G. Louie, *Phys. Rev. Lett.* **97**, 216803 (2006).
- 19) C. K. Gan and D. J. Srolovitz, *Phys. Rev. B* **81**, 125445 (2010).
- 20) S. K. Singh, M. Neek-Amal, and F. M. Peeters, *J. Chem. Phys.* **140**, 074304 (2014).
- 21) A. S. Barnard and I. K. Snook, *Model. Simul. Mater. Sci. Eng.* **19**, 054001 (2011).
- 22) J. Kang, O. L. Li, and N. Saito, *Carbon* **60**, 292 (2013).

- 23) G. Panomsuwan, S. Chiba, Y. Kaneko, N. Saito, and T. Ishizaki, *J. Mater. Chem. A* **2**, 18677 (2014).
- 24) D. Subramaniam, F. Libisch, Y. Li, C. Pauly, V. Geringer, R. Reiter, T. Mashoff, M. Liebmann, J. Burgdörfer, C. Busse, *et al.*, *Phys. Rev. Lett.* **108**, 046801 (2012).
- 25) C. M. Wettstein, F. P. Bonafé, M. B. Oviedo, and C. G. Sánchez, *J. Chem. Phys.* **144**, 224305 (2016).
- 26) S. Kim, S. W. Hwang, M.-K. Kim, D. Y. Shin, D. H. Shin, C. O. Kim, S. B. Yang, J. H. Park, E. Hwang, S.-H. Choi, *et al.*, *ACS Nano* **6**, 8203 (2012).
- 27) J. Lu, P. S. E. Yeo, C. K. Gan, P. Wu, and K. P. Loh, *Nat. Nanotechnol.* **6**, 247 (2011).
- 28) P. Leicht, L. Zielke, S. Bouvron, R. Moroni, E. Voloshina, L. Hammerschmidt, Y. S. Dedkov, and M. Fonin, *ACS Nano* **8**, 3735 (2014).
- 29) Y.-B. Tang, L.-C. Yin, Y. Yang, X.-H. Bo, Y.-L. Cao, H.-E. Wang, W.-J. Zhang, I. Bello, S.-T. Lee, H.-M. Cheng, *et al.*, *ACS Nano* **6**, 1970 (2012).
- 30) L. Zhao, M. Levendorf, S. Goncher, T. Schiros, L. Pálová, A. Zabet-Khosousi, K. T. Rim, C. Gutiérrez, D. Nordlund, C. Jaye, *et al.*, *Nano Letters* **13**, 4659 (2013).
- 31) H. J. Xiang, B. Huang, Z. Y. Li, S.-H. Wei, J. L. Yang, and X. G. Gong, *Phys. Rev. X* **2**, 011003 (2012).
- 32) P. Lambin, H. Amara, F. Ducastelle, and L. Henrard, *Phys. Rev. B* **86**, 045448 (2012).
- 33) T. Umeki, A. Akaishi, A. Ichikawa, and J. Nakamura, *J. Phys. Chem. C* **119**, 6288 (2015).
- 34) S. Yu, W. Zheng, Q. Wen, and Q. Jiang, *Carbon* **46**, 537 (2008).
- 35) Y. Li, Z. Zhou, P. Shen, and Z. Chen, *ACS Nano* **3**, 1952 (2009).
- 36) Y. Uchida, S.-i. Gomi, H. Matsuyama, A. Akaishi, and J. Nakamura, *J. Appl. Phys.* **120**, 214301 (2016).
- 37) P. v. R. Schleyer, *Chem. Rev.* **101**, 1115 (2001).
- 38) I. A. Popov, K. V. Bozhenko, and A. I. Boldyrev, *Nano Res.* **5**, 117 (2012).
- 39) M. Solà, *Front. Chem.* **1**, 22 (2013).
- 40) P. v. R. Schleyer, *Chem. Rev.* **105**, 3433 (2005).
- 41) E. Clar, *The Aromatic Sextet*, London, Wiley, (1972).
- 42) P. v. R. Schleyer, C. Maerker, A. Dransfeld, H. Jiao, and N. J. R. v. E. Hommes,

- J. Am. Chem. Soc. **118**, 6317 (1996).
- 43) D. Moran, F. Stahl, H. F. Bettinger, H. F. Schaefer, and P. v. R. Schleyer, J. Am. Chem. Soc. **125**, 6746 (2003).
- 44) Z. Chen, C. S. Wannere, C. Corminboeuf, R. Puchta, and P. v. R. Schleyer, Chem. Rev. **105**, 3842 (2005).
- 45) A. D. Zdetsis and E. N. Economou, J. Phys. Chem. C **119**, 16991 (2015).
- 46) J.-i. Aihara, J. Am. Chem. Soc. **128**, 2873 (2006).
- 47) J.-i. Aihara, M. Makino, and K. Sakamoto, J. Phys. Chem. A **117**, 10477 (2013).
- 48) K. Sakamoto, N. Nishina, T. Enoki, and J.-i. Aihara, J. Phys. Chem. A **118**, 3014 (2014).
- 49) N. Nishina, M. Makino, and J.-i. Aihara, J. Phys. Chem. A **120**, 2431 (2016).
- 50) W. Hu, L. Lin, C. Yang, and J. Yang, J. Chem. Phys. **141**, 214704 (2014).
- 51) M. J. Frisch, G. W. Trucks, H. B. Schlegel, G. E. Scuseria, M. A. Robb, J. R. Cheeseman, G. Scalmani, V. Barone, B. Mennucci, G. A. Petersson, *et al.*, *Gaussian 09, Revision D.01* (2009), Gaussian Inc. Wallingford CT 2009.
- 52) S. H. Vosko, L. Wilk, and M. Nusair, Can. J. Phys. **58**, 1200 (1980).
- 53) X. H. Zheng, X. L. Wang, T. A. Abtew, and Z. Zeng, J. Phys. Chem. C **114**, 4190 (2010).